JACS
JOURNAL OF THE AMERICAN CHEMICAL SOCIETY

Article

pubs.acs.org/JACS

# Atomic Level Resolution of Dye Regeneration in the Dye-Sensitized Solar Cell

Kiyoshi C. D. Robson,[†] Ke Hu,[‡] Gerald J. Meyer,*[,‡] and Curtis P. Berlinguette*[,†]

[†]Department of Chemistry and Centre for Advanced Solar Materials, University of Calgary, 2500 University Drive Northwest, Calgary T2N 1N4, Canada

[‡]Departments of Chemistry and Materials Science & Engineering, Johns Hopkins University, 3400 North Charles Street, Baltimore, Maryland 21218, United States

Supporting Information

**ABSTRACT:** Two donor–acceptor organic dyes have been synthesized that differ only by a two-heteroatom change from oxygen to sulfur within the donor unit. The two dyes, (*E*)-3-(5-(4-(bis(4-(hexyloxy)phenyl)amino)phenyl)thiophen-2-yl)-2-cyanoprop-2-enoic acid (**Dye-O**) and (*E*)-3-(5-(4-(bis(4-(hexylthio)phenyl)amino)phenyl)thiophen-2-yl)-2-cyanoprop-2-enoic acid) (**Dye-S**), were tested in solar cell devices employing both $I_3^-/I^-$-based and $[Co(bpy)_3]^{3+/2+}$ redox mediators. Power conversion efficiencies over 6% under simulated AM 1.5 illumination (1 Sun) were achieved in both electrolytes. Despite similar optical and redox properties for the two dyes, a consistently higher open-circuit voltage ($V_{oc}$) was measured for **Dye-S** relative to **Dye-O**. The improved efficiency observed with **Dye-S** in an iodide redox mediator is against the commonly held view that sulfur atoms promote charge recombination attributed to inner-sphere interactions. Detailed mechanistic studies revealed that this is a consequence of a 25-fold enhancement of the regeneration rate constant that enhances the regeneration yield under open circuit conditions. The data show that a high short circuit photocurrent does not imply optimal regeneration efficiency as is often assumed.

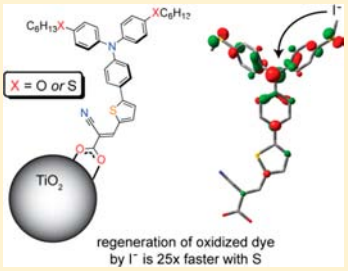


## INTRODUCTION

Dye-sensitized solar cells (DSSC) continue to be actively pursued as low cost alternatives to traditional photovoltaics.[1] The successful utilization of $Co^{III/II}$ diimine compounds as redox mediators[2−5] removes some of the inherent thermodynamic limitations of the $I_3^-/I^-$ mediators[6] and could soon enable a leapfrog jump in efficiency. Also impressive is the molecular detail in which DSSCs can now be optimized.[7,8] Isotopic substitution has also been shown to enhance excited-state electron injection yields.[9] Indeed, several recent reports demonstrate that exchange of a single atom, or a few atoms, in a dye molecule markedly changes the efficiencies of DSSCs comprised of them. While the magnitude of the efficiency change can be quite dramatic, the origin(s) generally remains speculative. Adducts comprised of one of the exchanged atoms with redox mediators present in the electrolyte are generally invoked to rationalize photoelectrochemical behavior.[10,11] In all cases investigated thus far, adduct formation lowers DSSC efficiencies. The findings disclosed herein suggest that adduct formation, most likely involving iodide activation, can result in enhanced power conversion efficiencies when the position of the exchanged atom within the dye structure is carefully taken into account.

One would indeed expect changes in DSSC efficiency when heteroatoms in a dye molecule are exchanged. Adduct formation between the dye and the semiconductor surface and/or species present in the electrolyte alters redox potentials and hence the interfacial electron-transfer kinetics that govern electrical power generation. O'Regan and Palomares have reported evidence of N–I and S–I binding.[10,12] The iodine species was thought to be the oxidized form of the redox mediator present in the electrolyte, either molecular iodine, $I_2$, or tri-iodide, $I_3^-$. The high surface concentration of these iodine-based electron acceptors at the $TiO_2$ interface results in conditions that favor unwanted charge recombination and hence lower the quasi-Fermi level of the illuminated $TiO_2$ thin film.[13] Based largely on this novel work, it is now widely accepted that the presence of sulfur heteroatom(s) in a dye molecule has a deleterious influence on energy conversion when employed in DSSCs. This conclusion is unfortunate as large classes of organic dye, such as polythiophenes and phenothiazines, possess S atoms.

To resolve the nature of these interactions, two oxygen atoms in the donor–acceptor organic dye (*E*)-3-(5-(4-(bis(4-(hexyloxy)-phenyl)amino)phenyl)thiophen-2-yl)-2-cyanoprop-2-enoic acid (**Dye-O**)[14] were replaced with two sulfur atoms, (*E*)-3-(5-(4-(bis(4-(hexylthio)phenyl)amino)phenyl)thiophen-2-yl)-2-cyano-prop-2-enoic acid) (**Dye-S**) shown in Figure 1. The dye molecules are "donor–acceptor" or "push–pull" type organic dyes wherein charge transfer occurs from the triphenylamine group (TPA) to the cyanoacetic acid moiety that can bind to the $TiO_2$. This orbital arrangement allows for efficient charge separation and vectorial electron transfer toward the $TiO_2$ surface subsequent to light absorption. Moreover, these donor and acceptor units are common modalities in high performance organic and/or inorganic DSSC sensitizers.[15−19]

**Received:** December 6, 2012
**Published:** January 10, 2013

   dx.doi.org/10.1021/ja311640f | *J. Am. Chem. Soc.* 2013, 135, 1961−1971

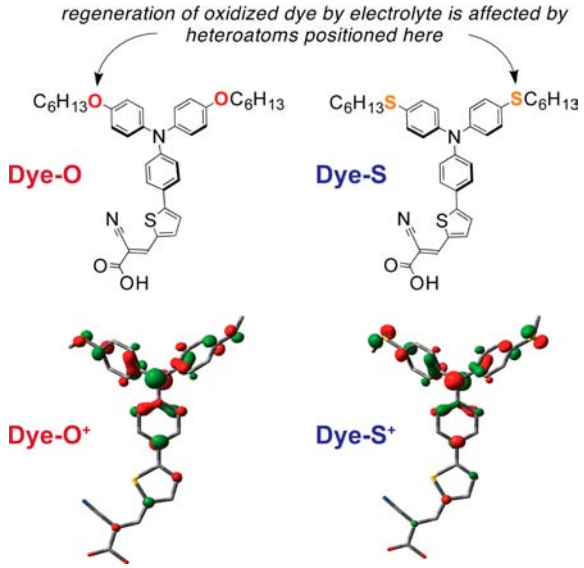


**Figure 1.** Molecular structures of the organic dyes **Dye-O** and **Dye-S**. The heteroatoms that have an effect on the regeneration reaction with redox mediators are indicated. The $\beta$-LUSO (lowest-unoccupied spin orbital) for the oxidized forms of each dye, **Dye-O**$^+$ and **Dye-S**$^+$, are provided below each structure to highlight the delocalization of the wave function onto the heteroatoms of interest (the terminal hexyl substituents were replaced with methyl substituents for the calculations).

In this study, the location of the substitution of the two-atom changes was carefully taken into consideration. As shown in Figure 1, there is a sizable orbital coefficient on the heteroatom (either O or S, for **Dye-O** and **Dye-S**, respectively) in the lowest-unoccupied spin orbital (LUSO) of the oxidized forms of the dyes (i.e., **Dye-O**$^+$ and **Dye-S**$^+$). Consequently, the delocalization of the LUSO onto the heteroatoms offers the opportunity to interrogate how S and O atoms can affect DSSC performance, particularly in view of the fact that it is this same portion of the oxidized sensitizer that directly interacts with the redox mediator. Comparative interfacial electron transfer studies were therefore conducted with **Dye-O** and **Dye-S** anchored to mesoporous $TiO_2$ thin films in the presence and absence of $Co^{III/II}$ and $I_3^-/I^-$ redox mediators. It is shown that the identity of the heteroatom can have a profound effect on dye regeneration, and in turn the open-circuit voltage ($V_{oc}$), as the S atoms enhance the rate of the reaction between the oxidized dye and the redox mediator by 3-fold with Co-based mediators, and 25-fold with iodide-based mediators.

## EXPERIMENTAL SECTION

**Preparation of Compounds.** All reactions and manipulations were performed using solvents passed through an MBraun solvent purification system prior to use. All reagents were purchased from Aldrich. Purification by column chromatography was carried out using silica (Silicycle: Ultrapure Flash Silica). Analytical thin-layer chromatography (TLC) was performed on aluminum-backed sheets precoated with silica 60 F254 adsorbent (0.25 mm thick; Merck, Germany) and visualized under UV light. Routine $^1$H and $^{13}$C NMR spectra were recorded at 400 and 100 MHz, respectively, on a Bruker AV 400 instrument at ambient temperature. Chemical shifts ($\delta$) are reported in parts per million (ppm) from low- to high-field and referenced to residual nondeuterated solvent in the Supporting Information. Standard abbreviations indicating multiplicity are used as follows: s = singlet; d = doublet; t = triplet; m = multiplet. All $^1$H chemical shifts follow the general labeling scheme in Figure 2. Organic and inorganic compounds **Dye-O**[14] and **P1-S**,[20] **P2-S**,[20] **P3-S**,[20] 4,4,5,5-tetramethyl-2-(thiophen-2-yl)-1,3,2-dioxaborolane,[21] 1,3-dimethylimidazolium iodide (DMII),[22] $[Co(bpy)_3](PF_6)_2$,[5] and $[Co(bpy)_3](PF_6)_3$[5] were synthesized according to literature reports.

**Substrate Preparations.** Mesoporous nanocrystalline $TiO_2$ thin films used in the spectroscopy studies were prepared as previously described.[23] Film thickness was determined to be about 5 $\mu$m by profilometry. The films were briefly immersed in acetonitrile solution containing dye (~75 $\mu$M) and coadsorbent chenodeoxycholic acid (~3.7 mM). Films were then washed with neat $CH_3CN$ and diagonally positioned in a standard 1 cm$^2$ quartz cuvette containing 0.5 M $LiClO_4$ acetonitrile solution. In some experiments, the sensitized thin films were sandwiched against a glass microscope with a vinyl film (Warps, 8 mil Vinyl-Pane) spacer that contained desired concentrations of $Co(bpy)_3^{2+}$ or LiI in 0.5 M $LiClO_4$ acetonitrile solutions. The electrolyte solutions were purged with Ar gas for at least 30 min prior to experimentation.

**Spectroelectrochemistry.** Steady-state UV–visible absorption spectra were obtained on a Varian Cary 50 spectrophotometer at room temperature. A potentiostat (BAS model CV-50W) was employed for measurements in a standard three-electrode arrangement with a sensitized $TiO_2$ thin film deposited on a FTO substrate working electrode, a platinum disk counter electrode, and a Ag/AgCl reference electrode (Bioanalytical Scientific Instruments, Inc.) in 0.5 M $LiClO_4$ acetonitrile solution. All potentials are reported versus the normal hydrogen electrode (NHE). The ferrocenium/ferrocene half-wave potential was measured at room temperature before and after each

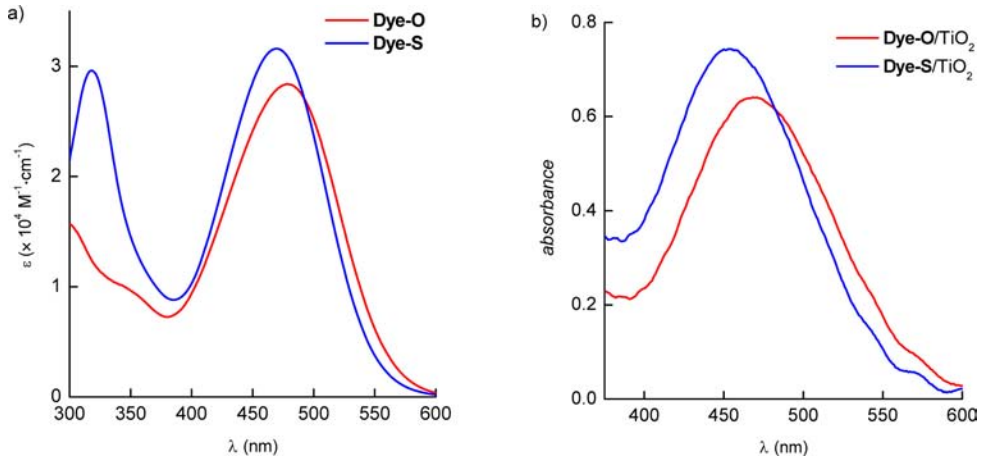


**Figure 2.** UV–vis absorption spectra of **Dye-O** (red) and **Dye-S** (blue) in (a) fluid $CH_3CN$ solution and (b) anchored to $TiO_2$ immersed in $CH_3CN$ solution at 298 K.


dx.doi.org/10.1021/ja311640f | J. Am. Chem. Soc. 2013, 135, 1961–1971

experiment and was used as an external standard to calibrate the reference electrode. Conversion constant of −640 mV from NHE to $Fc^+/Fc$ was used in acetonitrile at 25 °C.

**Transient Absorption Spectroscopy.** Nanosecond transient absorption measurements were obtained with an apparatus similar to that which has been previously described.[23] Briefly, samples were excited by a frequency doubled Q-switched, pulsed Nd:YAG laser (Quantel USA (BigSky) Brilliant B; 532 nm, 5−6 ns full width at half-maximum (fwhm), 1 Hz, ∼10 mm in diameter) directed 45° to the film surface. A Glan-Taylor polarizer was employed in the laser path to attenuate the pulse fluence. A 150 W xenon arc lamp coupled to a 1/4 m monochromator (Spectral Energy, Corp. GM 252) served as the probe beam (Applied Photophysics) that was aligned orthogonally to the excitation light. For detection at sub-100 μs time scales, the lamp was pulsed with 80 V. Detection was achieved with a monochromator (Spex 1702/04) optically coupled to an R928 photomultiplier tube (Hamamatsu). Transient data were acquired on a computer-interfaced digital oscilloscope (LeCroy 9450, Dual 350 MHz) with 2.5 ns resolution terminated at 50 Ω for sub-100 μs; for longer time scales, the signal was terminated with a 10 kΩ resistor and bandwidth limited at 80 MHz. Typically, 30−50 laser pulses were averaged at each observation wavelength over the range 380−710 nm for full spectra generation. 300−500 laser pulses were typical averages for single wavelength measurement to achieve satisfactory S/N. Kinetic data fitting and spectral modeling was performed in Origin 8, and least-squares error minimization was accomplished using the Levenberg−Marquardt iteration method.

**DFT Calculations.** Density functional theory (DFT) calculations were carried out using B3LYP and the 6-31G(d) basis set. All geometries were fully optimized in the ground states (closed shell) and the +1 oxidized states (open shell). Time-dependent density functional theory (TD-DFT) calculations were performed with an IEFPCM solvation model ($CH_3CN$) using a spin-restricted formalism to examine low-energy excitations at the ground-state geometry. All calculations were carried out with the Gaussian 03W software package.[24]

**Cell Fabrication.** Photoanodes were prefabricated by Dyesol Inc. (Australia) with screen-printable $TiO_2$ pastes (18-NRT and WER4-O, Dyesol). The active area of the $TiO_2$ electrodes was 0.28 $cm^2$ with a thickness of 6 μm (18-NRT) and 3 μm (WER4-O) on fluorine-doped tin-oxide [FTO; TEC8 (8 Ω $cm^{-2}$)]. The $TiO_2$ substrates were treated with $TiCl_4$(aq) (0.05 M) at 70 °C for 30 min and subsequently rinsed with $H_2O$ and then dried prior to heating. The electrodes were heated to 450 °C for 20 min in an ambient atmosphere and left to cool to 80 °C prior to immersing into an acetonitrile solution containing the dye (∼0.25 mM) and chenodeoxycholic acid (∼2.5 mM) for 16 h. The stained films were then rinsed with copious amounts of $CH_3CN$ and dried. The cells were fabricated using Pt-coated counter-electrode [FTO TEC-15 (15 Ω $cm^{-2}$)] and sealed with a 30 μm Surlyn (Dupont) gasket by resistive heating. Two electrolytes were used for this study: (i) $I_3^-/I^-$ [1.0 M 1,3-dimethylimidazolium iodide (DMII), 60 mM $I_2$, 0.5 M *tert*-butylpyridine, 0.05 M NaI, and 0.1 M GuNCS in a mixed solvent system of acetonitrile and valeronitrile (85:15, v/v)]; (ii) $Co^{III/II}$ [0.21 M $[Co(bpy)_3](PF_6)_2$,0.033 M $[Co(bpy)_3](PF_6)_3$, 0.1 M $NaClO_4$, and 0.2 M *tert*-butylpyridine in acetonitrile]. Each electrolyte was introduced into the two sandwiched electrodes via vacuum backfilling through a hole in the counter electrode. In the cases where the $I_3^-/I^-$ electrolyte was used, the hole was sealed with an aluminum-backed Bynel foil (Dyesol). In the cases where the $Co^{III/II}$ electrolyte was used, the hole was covered with a thin Surlyn (25 μm) microscope slide; aluminum foil was then taped to the back of the cell. Silver bus bars were added to all cells after sealing.

**Cell Characterization.** Photovoltaic measurements were recorded with a Newport Oriel solar simulator (model 9225A1) equipped with a class A 150 W xenon light source powered by a Newport power supply (model 69907). The light output (area = 5 cm × 5 cm) was calibrated to AM 1.5 using a Newport Oriel correction filter to reduce the spectral mismatch in the region of 350−700 nm to less than 1.5%. The power output of the lamp was measured to 1 Sun (100 mW $cm^{-2}$) using a certified Si reference cell. The current−voltage ($I$−$V$) characteristic of each cell was obtained by applying an external potential bias to the cell and measuring the generated photocurrent with a Keithley digital source meter (model 2400). All cells were measured with a mask size of 0.13 $cm^2$. IPCE measurements were performed on a QEX7 Solar Cell Spectral Response Measurement System from PV Instruments, Inc. The system was calibrated with a photodiode that was calibrated against NIST standard I755 with a transfer uncertainty of less than 0.5% between 400 and 1000 nm, and less than 1% at all other wavelengths. All measurements were made in AC mode at a 10 Hz chopping frequency under a bias light. The system was calibrated and operated in Beam Power mode.

## RESULTS

**Synthesis and Characterization.** The preparation of **Dye-O** followed a previously reported literature procedure.[14] A similar protocol was followed for **Dye-S** with the exception of the generation of the **P2-S** precursor, which was isolated following an electrophilic aromatic substitution reaction between **P1-S** and $C_6H_{13}S^-$ (Scheme S1, Supporting Information). A subsequent electrophilic bromination step with NBS furnished the bromoderivative **P3-S**, which could undergo reaction with 4,4,5,5-tetramethyl-2-(thiophen-2-yl)-1,3,2-dioxaborolane under Suzuki cross-coupling conditions to yield **P4-S**. A Vislmeier−Haack formylation was employed to install the −CHO group (**P5-S**), which was condensed with cyanoacetic acid to yield the target **Dye-S**.

The optical spectra of **Dye-O** and **Dye-S** recorded in $CH_3CN$ are very similar, Figure 2a. **Dye-O** is characterized by an intense charge-transfer absorption band centered at $\lambda_{max}$ = 478 nm ($\varepsilon$ = 2.84 × $10^4$ $M^{-1}$ $cm^{-1}$), while that of **Dye-S** is slightly hypsochromically shifted to $\lambda_{max}$ = 470 nm ($\varepsilon$ = 3.16 × $10^4$ $M^{-1}$ $cm^{-1}$). The slight differences in absorption are attributed to less orbital overlap of the sulfur lone pairs with the $\pi$ system of the aryl rings of the TPA groups relative to those of the oxygen atoms, which was corroborated by the $^1$H NMR chemical shifts and redox chemistry (vide infra) of the two complexes.[20] Time-dependent DFT indicates that, for both **Dye-O** and **Dye-S**, the HOMO, HOMO−1, and HOMO−2 orbitals are localized to the electron-rich TPA moiety, and the LUMO and LUMO+1 levels are confined to the cyanoacetic acid portion of the molecule; the lowest energy transition (Figures S2 and S3) is a LUMO ← HOMO transition. Light excitation into the charge transfer absorption bands resulted in room temperature fluorescence (Figure S4).

The dyes were found to bind to thin films of anatase, mesoporous $TiO_2$ with high surface coverages over 1 × $10^{-7}$ mol/$cm^2$, and are herein abbreviated **Dye-O**/$TiO_2$ and **Dye-S**/$TiO_2$. When the sensitized thin films were measured in neat $CH_3CN$, the absorption maxima were slightly blue-shifted from that observed in fluid solution, Figure 2. The presence of 0.5 M $LiClO_4$ induced a significant bathochromic (red) shift in both cases, measured to be 870 $cm^{-1}$ for **Dye-O**/$TiO_2$ and 750 $cm^{-1}$ for **Dye-S**/$TiO_2$ (Figure S5). Lewis acidic cations, such as $Li^+$ and $Na^+$, bind to anatase $TiO_2$, and the local field generated is known to induce a bathochromic shift of dye molecules anchored to the same surface.[25]

The cyclic voltammograms of **Dye-O** or **Dye-S** in 0.1 M $NBu_4BF_4/CH_3CN$ electrolyte displayed quasi-reversible $TPA^{\bullet+}/TPA^0$ redox waves at +0.96 and +1.06 V vs NHE, respectively (Figure S6). Cyclic voltammetry of the sensitized thin films showed broad waves with large peak-to-peak splittings (Figure S7). Spectroelectrochemistry was therefore used to estimate the reduction potentials of **Dye-O**/$TiO_2$ and **Dye-S**/$TiO_2$. Oxidation of **Dye-O**/$TiO_2$ or **Dye-S**/$TiO_2$ resulted in characteristic absorption changes attributed to the oxidized triphenylamine, Figure 3. Isosbestic points were maintained, and the spectral changes were reversible upon stepping the potential back to less positive values.


dx.doi.org/10.1021/ja311640f | J. Am. Chem. Soc. 2013, 135, 1961−1971

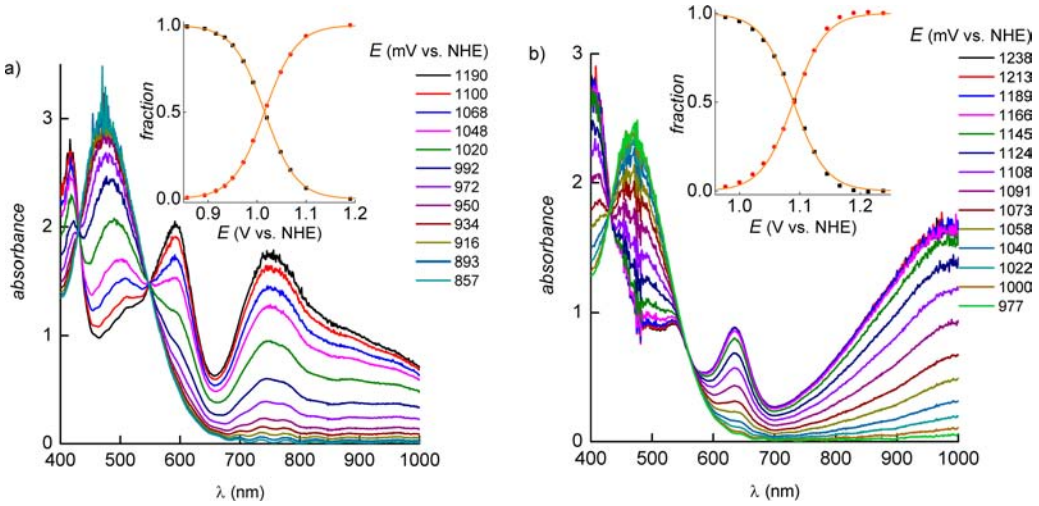


**Figure 3.** Visible absorption spectra of (a) **Dye-O**/$TiO_2$ (dye surface coverage $\Gamma = 1.0 \times 10^{-8}$ mol $cm^{-2}$) and (b) **Dye-S**/$TiO_2$ ($\Gamma = 5.3 \times 10^{-8}$ mol $cm^{-2}$) measured at the indicated applied potentials in 0.5 M $LiClO_4$ $CH_3CN$ solution. The insets show the fraction ($x$) of dye molecules present in the reduced (■) and the oxidized state (red ●). Overlaid on this data is a sigmoidal fit, $x = 1/(1 + 10\exp((E_{app} - E^\circ_{1/2})/a \times 59\text{ mV}))$, where $a$ is the ideality factor determined to be 1.27 for **Dye-O**/$TiO_2$ and 1.05 for **Dye-S**/$TiO_2$.

The insets of Figure 3 show the fraction of molecules in each oxidation state as a function of applied potential, $E_{app}$. This fraction of ($x$) was calculated by $x = 1/(1 + 10\exp((E_{app} - E^\circ)/a \times 59\text{ mV}))$. The formal reduction potential, $E^\circ$, was taken as the equilibrium potential where the fraction present was 0.5, and was measured to be +1090 mV vs NHE for **Dye-S**/$TiO_2$ while +1015 mV for **Dye-O**/$TiO_2$. Ideality factors of $a = 1.27$ for **Dye-O**/$TiO_2$ and $a = 1.05$ for **Dye-S**/$TiO_2$ were required to fit the data.[13] In some cases, the fractional surface coverage was converted to a chemical capacitance in units of mF/$cm^2$ by $(-dx/dE_{app}) \times \Gamma \times \mathcal{F} \times 10^6$, where $\Gamma$ is the surface coverage in mol/$cm^2$ and $\mathcal{F}$ is Faraday's constant (96 485 C $mol^{-1}$).

The $E_{0-0}$ energy was calculated to be 2.31 and 2.32 eV for **Dye-O** and **Dye-S**, respectively, from the intersection of the absorption and fluorescence spectra (Table 1 and Figure S4). The excited-state reduction potential, $E(S^+/S^*)$, was then calculated by $E(S^+/S^*) = E(S^+/S) - E_{0-0}$ to be −1.35 and −1.26 V vs NHE for **Dye-O** and **Dye-S**, respectively.

The application of negative applied potentials to the sensitized thin films immersed in 0.5 M $LiClO_4/CH_3CN$ resulted in reduction of $TiO_2$ and the characteristic absorption of the trapped $TiO_2$ electron, $TiO_2(e^-)$. The potential dependence of this reduction was found to be the same for **Dye-O**/$TiO_2$ and **Dye-S**/$TiO_2$, and was well described by a single exponential fit (Figure S8). The measured absorbance was related to the number of $TiO_2(e^-)$'s per 15 nm diameter spherical particle through Beer's law and the extinction coefficient $\varepsilon = 1000$ $M^{-1}$ $cm^{-1}$ with an effective optical path length for a 5 $\mu$m thick film of 50% porosity positioned 45° to the probe light. For example, the absorption due to 20 electrons per particle was calculated as $\text{Abs} = \varepsilon \cdot b \cdot c(TiO_2(e^-)) = 1000\ (M^{-1}\ cm^{-1}) \times 5\ (\mu m) \times 1.414 \times 10^{-4}\ (cm\ \mu m^{-1}) \times 50\% \times 20/(4/3 \times \pi \times (7.5 \times 10^{-9}(m))^3 \times N_A/10^3(L\ m^{-3})) = 0.007$.

**Interfacial Charge Recombination.** Nanosecond transient absorption spectroscopy was used to quantify interfacial electron transfer from $TiO_2$ to the oxidized sensitizers. Absorption difference spectra of **Dye-O**/$TiO_2$ and **Dye-S**/$TiO_2$ displayed in Figure 4 were acquired in 0.5 M $LiClO_4$ $CH_3CN$ after pulsed 532 nm excitation of the sensitized thin films. Simulations based on a 1:1 stoichiometry of oxidized dyes and injected electrons,

**Table 1. Summary of Spectroscopic and Electrochemical Properties for Dye-O and Dye-S in Solution and Anchored to $TiO_2$**

| compound | $\lambda_{max}$ (nm)[a] | $\lambda_{PL}$ (nm)[b] | $E_{1/2}$ (V vs NHE)[c] | $E_{0-0}$ (eV)[d] | $E(S^+/S^*)$ (V vs NHE)[e] |
|---|---|---|---|---|---|
| **Dye-O** | 478 (2.84) | 598 | 0.96 | 2.31 | −1.35 |
| **Dye-O**/$TiO_2$ | 468 | | 1.02 | 2.03 | −1.01 |
| **Dye-S** | 469 (3.16), 318 (2.96) | 623 | 1.06 | 2.32 | −1.26 |
| **Dye-S**/$TiO_2$ | 453 | | 1.09 | 2.12 | −1.03 |

[a]Corresponds to maximum of lowest-energy absorption band recorded in $CH_3CN$; $\varepsilon$ values indicated in parentheses with units of $\times 10^4$ $M^{-1}$ $cm^{-1}$. [b]Fluorescence maxima determined in $CH_3CN$ after excitation at a wavelength corresponding to $\lambda_{max}$. [c]Corresponds to $TPA^{\bullet+}/TPA^0$ redox couple. Data collected in 0.1 M $NBu_4BF_4$ $CH_3CN$ solutions at 100 mV/s and referenced to $[Fc]^+/[Fc]$ (+640 mV vs NHE). Data for sensitized $TiO_2$ thin films were collected in 0.5 M $LiClO_4$ $CH_3CN$ solutions by density of states measurements (see Figure 11). [d]In fluid solution, $E_{0-0}$ was estimated from the intersection of the normalized absorption and fluorescence spectra (see Figure S4). For the sensitized $TiO_2$ thin films, $E_{0-0}$ was estimated from the intercept of a tangent line drawn on the red edge of ground-state absorption. [e]Estimated using $E(S^+/S^*) = E_{1/2} - E_{0-0}$.

**Dye**$^+$/$TiO_2(e^-)$, plus the first derivative of the ground-state absorption were in good agreement with the experimental data. Normalization of the measured spectra at different observation times revealed that the bleach in the initial spectra was red-shifted relative to those observed at longer delay times. The first derivative absorption feature is consistent with previous studies and the presence of an underlying electric field that influences the sensitizer absorption spectra in a manner similar to that observed in Stark spectroscopy. The time-dependent spectral changes are due to screening of the electric field by solvents and ions.[25,26] The immediate appearance of the absorption spectrum of the oxidized dye molecule indicated that electron injection occurred with a rate constant $k_{inj} > 10^8$ $s^{-1}$.

Shown in Figure 5 are absorption changes measured after pulsed light excitation of **Dye-O**/$TiO_2$ and **Dye-S**/$TiO_2$ in 0.5 M $LiClO_4/CH_3CN$ that correspond to charge recombination between the injected electron and the oxidized sensitizer. Both sensitized thin films had a ground-state absorption of 0.43 at the


dx.doi.org/10.1021/ja311640f | J. Am. Chem. Soc. 2013, 135, 1961−1971

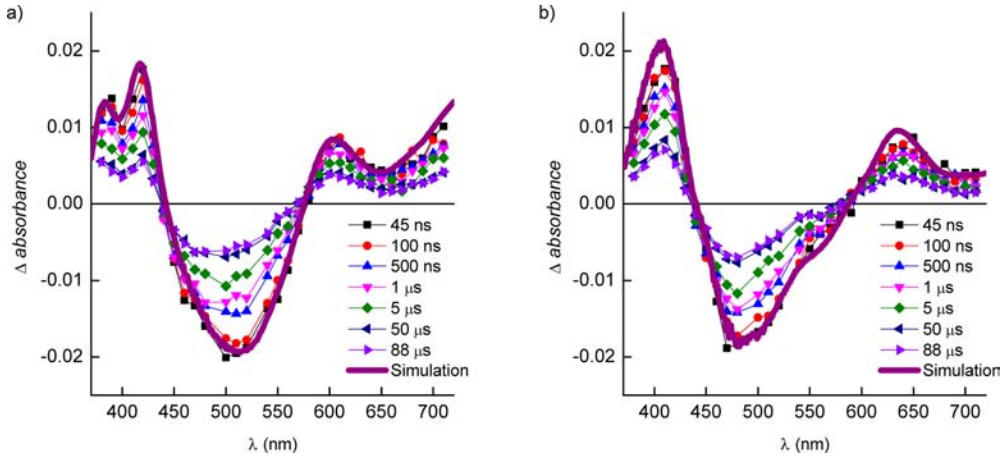


**Figure 4.** Absorption difference spectra measured at the indicated delay times after pulsed 532 nm excitation of (a) **Dye-O**/$TiO_2$ and (b) **Dye-S**/$TiO_2$ immersed in 0.5 M $LiClO_4/CH_3CN$ solution. Overlaid in purple are simulated spectra.

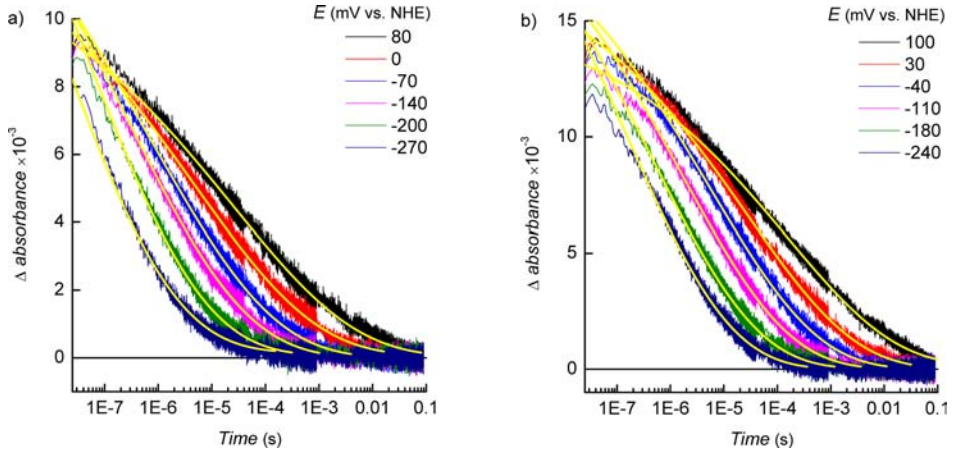


**Figure 5.** Absorption change monitored at 635 nm after pulsed light excitation (532 nm; laser fluence: 0.3 mJ/$cm^2$) of **Dye-O**/$TiO_2$ (left) and **Dye-S**/$TiO_2$ (right) immersed in 0.5 M $LiClO_4/CH_3CN$ at the indicated applied potentials. Overlaid in yellow are best fits to the KWW kinetic model.

532 nm excitation wavelength. The kinetics were nonexponential but were satisfactorily modeled by Kohlrausch–Williams–Watts (KWW) function, eq 1, with a $\beta$ value of 0.20 ± 0.01 for both sensitizers on mesoporous nanocrystalline $TiO_2$ surface.[27] Average charge recombination rate constants, $k_{cr}$, were calculated as the first moment[28] of the underlying Lévy distribution of rate constants, eq 2.

$$\Delta\text{Abs} = A \exp[-(kt)^{\beta}] \quad (1)$$

$$k_{cr} = \left[\frac{1}{k\beta} \times \Gamma\left(\frac{1}{\beta}\right)\right]^{-1} \quad (2)$$

The rate constants were found to be within experimental error the same, $k_{cr} = 1.3 \pm 0.1 \times 10^2$ $s^{-1}$ for **Dye-O**/$TiO_2$ and $k_{cr} = 1.4 \pm 0.1 \times 10^2$ $s^{-1}$ for **Dye-S**/$TiO_2$ (Figure S9). The reduction of $TiO_2$ with forward bias had a marked influence on the average charge recombination rate constants as is shown in Figure 5. The $k_{cr}$ values were found to increase exponentially with the applied potential from +100 to −300 mV vs NHE (Figure S10).

The $V_{oc}$ was measured in the absence of redox mediator under the same condition as the charge recombination measurement described previously. Over 2 decades of irradiances, the $V_{oc}$ values for **Dye-O**/$TiO_2$ and **Dye-S**/$TiO_2$ were within experimental error the same (Figure S11).

**Sensitizer Regeneration.** The regeneration of **Dye-O**$^+$/$TiO_2(e^-)$ and **Dye-S**$^+$/$TiO_2(e^-)$ by iodide and $[Co(bpy)_3]^{2+}$ donors was investigated. A laser pulse was used to generate the interfacial charge separated state, **Dye-O**$^+$/$TiO_2(e^-)$ or **Dye-S**$^+$/$TiO_2(e^-)$, in an electrolyte that contained known amounts of $I^-$ or $[Co(bpy)_3]^{2+}$. The data were recorded at an observation wavelength of 635 nm where the oxidized dye predominantly absorbed light, Figure 6. The observed kinetic data could not be fit to a single exponential function, but were adequately described by a sum of two exponential functions, from which an average rate constant was calculated, eqs 3 and 4.

$$\Delta\text{Abs} = A_0 + A_1 \exp(-k_1 t) + A_2 \exp(-k_2 t) \quad (3)$$

$$\bar{k}_{obs} = \frac{A_1/k_1 + A_2/k_2}{A_1/k_1^2 + A_2/k_2^2} \quad (4)$$

The $\bar{k}_{obs}$ values were linear in the $Co(bpy)_3^{2+}$ and $I^-$ as is shown in Figure 7. The slopes from the linear fits provided the second-order rate constants for dye regeneration. The values are summarized in Table 2.

The regeneration efficiency, $\phi_{reg}$, was quantified on the basis of the charge recombination and regeneration rate constants, eq 5:

$$\phi_{reg} = k_{reg}[D]/(k_{cr} + k_{reg}[D]) \quad (5)$$


dx.doi.org/10.1021/ja311640f | J. Am. Chem. Soc. 2013, 135, 1961−1971

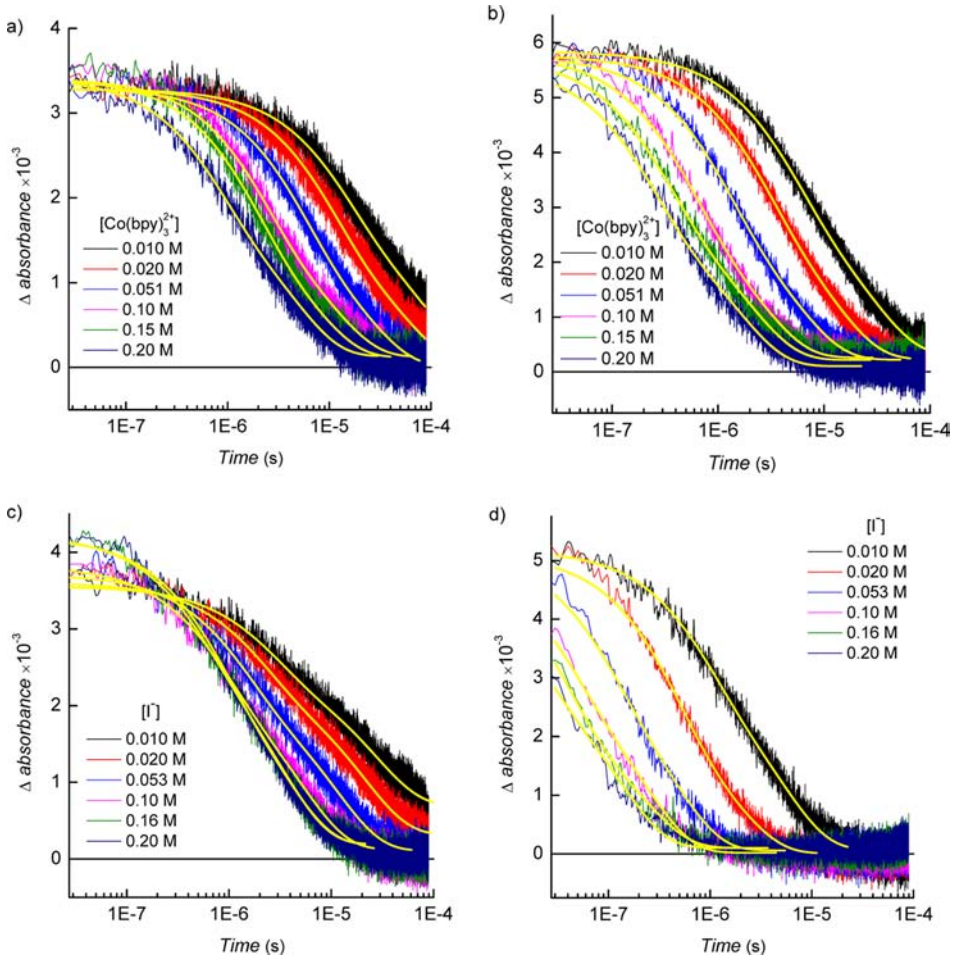


**Figure 6.** Absorption changes measured after pulsed laser excitation of the sensitized film in the presence of the indicated concentration of $[Co(bpy)_3](ClO_4)_2$, (a) **Dye-O**/$TiO_2$ and (b) **Dye-S**/$TiO_2$, or LiI, (c) **Dye-O**/$TiO_2$ and (d) **Dye-S**/$TiO_2$ in 0.5 M $LiClO_4/CH_3CN$. Absorbance changes were monitored at a probe wavelength of 635 nm (excitation wavelength, 532 nm; laser fluence, 0.1 mJ/$cm^2$). Overlaid in yellow are the best fits to biexponential kinetic model.

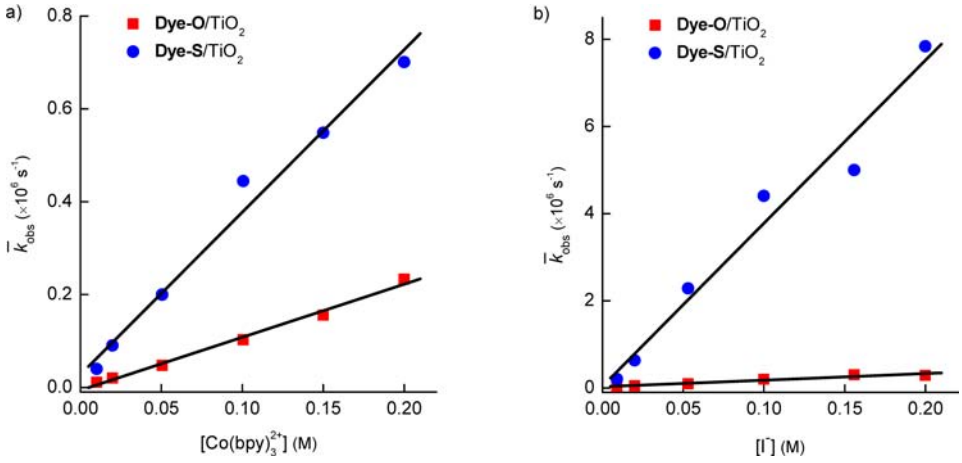


**Figure 7.** Plots of observed regeneration rate constants ($\bar{k}_{obs}$) of **Dye-O**/$TiO_2$ (red ■) and **Dye-S**/$TiO_2$ (blue ●) obtained from the kinetics fits versus titrated (a) $[Co(bpy_3]^{2+}$ and (b) $[I^-]$ concentrations.

where $D$ is the donor concentration. The $\phi_{reg}$ values reflect the facts that charge recombination rate constants were highly sensitive to the extent of forward bias and that regeneration rate constants were larger for **Dye-S**$^+$/$TiO_2(e^-)$, Table 3.

Transient absorption spectra were also recorded after pulsed laser excitation in the presence of iodide. At long observation times (>10 $\mu$s), the injected electron and $I_3^-$ were observed as well as a derivative feature attributed to a shift in the ground-state absorption of the dye molecules due to the injected electrons (an electroabsorption or Stark effect)[25,26] (Figure S12). Recombination of the injected electron with $I_3^-$ was found to be well modeled by KWW function with a $\beta$ value of 0.8 (Figure S13).


dx.doi.org/10.1021/ja311640f | J. Am. Chem. Soc. 2013, 135, 1961−1971

**Table 2. Second-Order Regeneration Rate Constants ($k_{reg}$) Abstracted for Dye-O/$TiO_2$ and Dye-S/$TiO_2$ in 0.5 M $LiClO_4$/$CH_3CN$ Containing Cobalt- and Iodide-Based Redox Mediators**

| | $[Co(bpy)_3]^{2+}$ | | iodide | | |
|---|---|---|---|---|---|
| | $k_{reg}$ ($M^{-1}s^{-1}$) | $\Delta G^{o\,a}$ (V) | $k_{reg}$ ($M^{-1}s^{-1}$) | $\Delta G^{o\,b}$ (V) | $\Delta G^{o\,c}$ (V) |
| **Dye-O**/$TiO_2$ | $1.1 \times 10^6$ | −0.46 | $1.5 \times 10^6$ | 0.21 | −0.09 |
| **Dye-S**/$TiO_2$ | $3.5 \times 10^6$ | −0.53 | $3.7 \times 10^7$ | 0.14 | −0.16 |

[a] $E°([Co(bpy)_3]^{3+/2+})$ = 0.56 V vs NHE. [b] Calculated free energy change for outer-sphere reactions based on $E°(I/I^-)$ = 1.23 V vs NHE. [c] Calculated free energy change for outer-sphere reactions based on $E°(I_2^{\bullet-}/2I^-)$ = 0.93 V vs NHE.

**Table 3. Regeneration Efficiencies Calculated by Equation 5 at the Indicated Forward Bias Conditions**

| | bias (mV vs NHE) | $\phi_{reg}$ 0.5 M $I^-$ | $\phi_{reg}$ 0.2 M $[Co^{II}(bpy)_3]^{2+}$ |
|---|---|---|---|
| **Dye-O**/$TiO_2$ | 80 | 1.0 | 1.0 |
| | 0 | 1.0 | 1.0 |
| | −70 | 0.99 | 0.97 |
| | −140 | 0.97 | 0.91 |
| | −200 | 0.83 | 0.60 |
| | −270 | 0.57 | 0.28 |
| **Dye-S**/$TiO_2$ | 100 | 1.0 | 1.0 |
| | 30 | 1.0 | 1.0 |
| | −40 | 1.0 | 1.0 |
| | −110 | 0.99 | 0.99 |
| | −180 | 0.99 | 0.95 |
| | −240 | 0.99 | 0.85 |

An average rate constant was calculated to be 2.3 ± 0.4 $s^{-1}$ with eq 2.

At short observation times, there was clear kinetic evidence for the presence of $I_2^{\bullet-}$. It was of interest to test whether injected electrons recombined with $I_2^{\bullet-}$. This was accomplished by a method that was previously described.[29] The absorption change at 396 nm, where both $I_3^-$ and $I_2^{\bullet-}$ absorbed light, was measured at a sufficiently long delay time (10 $\mu$s) to ensure that all of the photogenerated $I_2^{\bullet-}$ had disproportionated. The initial amplitude of the absorption change expected if quantitative $I_2^{\bullet-}$ disproportionation occurred was then calculated, based on the known relative extinction coefficients of $I_3^-$ and $I_2^{\bullet-}$,[29] and compared to the experimentally measured value. After a small correction for contributions from the oxidized dye, the calculated and experimentally measured values were within experimental error the same for **Dye-S**/$TiO_2$, consistent with quantitative $I_2^{\bullet-}$ disproportionation (Figure S14). In other words, all of the $I_2^{\bullet-}$ that was photogenerated underwent disproportionation with no evidence for a $TiO_2(e^-) + I_2^{\bullet-} \rightarrow$ reaction. This same conclusion could not be reached for **Dye-O**/$TiO_2$ due to the more sluggish regeneration rates that made kinetic analysis difficult.

**Light-to-Electrical Energy Conversion.** Photocurrent density−voltage plots are shown for DSSCs with **Dye-O** and **Dye-S** using an iodide- and cobalt-based electrolytes, Figure 8. The DSSCs fabricated with **Dye-S** display power conversion efficiencies ($\eta$) similar to those fabricated with **1** with the $I_3^-/I^-$-based electrolytes, Table 4. The DSSCs fabricated with **Dye-O** and **Dye-S** and an $I_3^-/I^-$-based electrolyte displayed PCEs of 6.1 ± 0.2% and 6.2 ± 0.3%, respectively. The DSSCs fabricated with **Dye-O** or **Dye-S** and the $Co^{III/II}$ redox mediator displayed $\eta$ of 4.6 ± 0.4% and 6.3 ± 0.7%, respectively.

Photocurrent action spectra, measured as the incident photon-to-current efficiency (IPCE) versus wavelength shown in Figure 9, were in good agreement with the absorptance spectra. The slight decrease in photocurrent efficiency that was measured below 420 nm with the iodide containing electrolyte is due to competitive light absorption by tri-iodide. The **Dye-O** absorbed light to about 650 nm. When corrections were made for light scattering and absorption by the FTO substrate, the efficiency was near 100%.

## DISCUSSION

The two dyes investigated in this study, which differ only by a two-heteroatom change from oxygen to sulfur within the donor unit, revealed nearly quantitative short-circuit photocurrent efficiencies when employed in DCCS with iodide or cobalt redox mediators. However, the open circuit photovoltage, $V_{oc}$, was found to be largest for **Dye-S** under all conditions investigated. It is not the absolute values of the conversion efficiencies that are novel in this study as Wang et al. have reported more optimal data,[14] and even higher values for structurally related organic dyes have been realized by Bai and co-workers.[30] Instead, this comparative study revealed an improvement with **Dye-S** that stands in stark contrast to the commonly accepted view that sulfur atoms incorporated within the organic framework of a dye molecule enhance recombination and hence lower the overall light-to-electrical energy conversion efficiency. In fact, recombination of the injected electrons with the oxidized dye was within experimental error the same for the two sensitized materials.

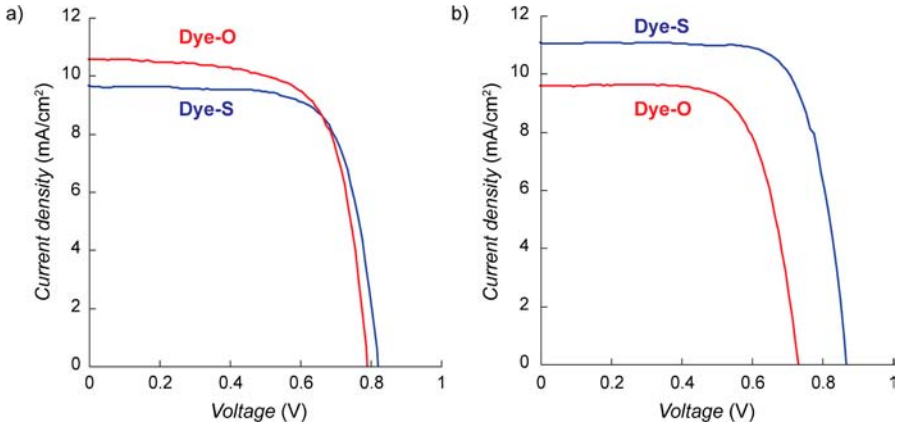


**Figure 8.** Current−voltage curves for DSSCs fabricated with **Dye-O** and **Dye-S** at AM1.5 illumination using (A) $I_3^-/I^-$ and (B) $Co^{III/II}$ redox mediators.


dx.doi.org/10.1021/ja311640f | J. Am. Chem. Soc. 2013, 135, 1961−1971

**Table 4. Solar Cell Performance Parameters Obtained under Simulated AM 1.5 Illumination (1 Sun) for Dye-O and Dye-S**

| compound | electrolyte[a] | $J_{sc}$ (mA/cm$^2$) | $V_{oc}$ (mV) | fill factor | $\eta$ (%)[b] |
|---|---|---|---|---|---|
| **Dye-O** | $I^-/I_3^-$ | 11.7 ± 0.2 | 734 ± 21 | 70.5 ± 1.5 | 6.1 ± 0.2 |
| **Dye-S** | $I^-/I_3^-$ | 10.3 ± 0.6 | 798 ± 24 | 74.4 ± 2.2 | 6.2 ± 0.3 |
| **Dye-O** | $Co^{III/II}$ | 10.1 ± 0.5 | 714 ± 31 | 63.7 ± 4.8 | 4.6 ± 0.4 |
| **Dye-S** | $Co^{III/II}$ | 10.8 ± 0.4 | 828 ± 38 | 70.0 ± 3.6 | 6.3 ± 0.7 |

[a]The $I_3^-/I^-$ electrolyte solution is composed of 1.0 M 1,3-dimethylimidazolium iodide (DMII), 60 mM $I_2$, 0.5 M *tert*-butylpyridine, 0.05 M NaI, and 0.1 M GuNCS in a mixed solvent system of acetonitrile and valeronitrile (85:15, v/v), while the $Co^{III/II}$ electrolyte is composed of 0.21 M $[Co(bpy)_3](PF_6)_2$, 0.033 M $[Co(bpy)_3](PF_6)_3$, 0.1 M $NaClO_4$, and 0.2 M *tert*-butylpyridine in acetonitrile. [b]A 0.13 cm$^2$ mask was used; averaged parameters, with standard deviations, from no fewer than three different cells are listed.

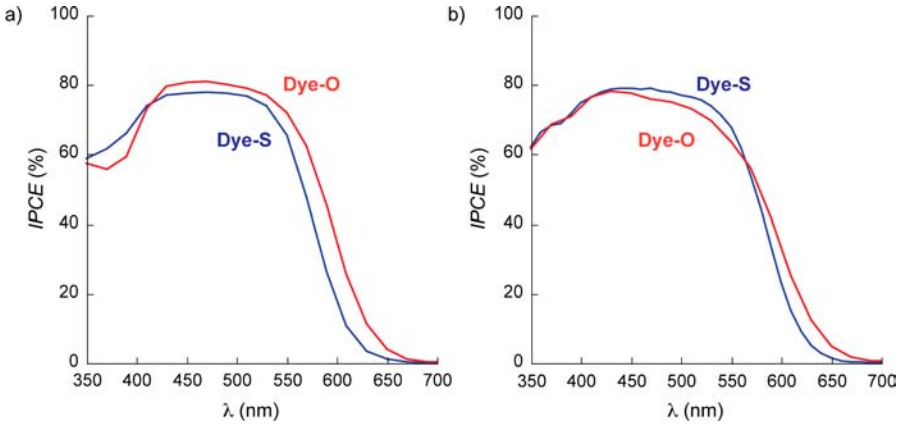


**Figure 9.** Incident-photon-to-current efficiency (IPCE) for DSSCs fabricated using (a) $I_3^-/I^-$ and (b) $Co^{III/II}$ redox mediators.

Likewise, recombination of injected electrons with oxidized iodide ions was also sensitizer independent. Surprisingly, the origin of the disparate $V_{oc}$ values was instead traced to an enhanced regeneration rate and efficiency for **Dye-S**. Detailed mechanistic studies revealed that regeneration was optimal at the short circuit condition for both dye molecules, but was not rapid enough for **Dye-O** to compete with **Dye-O**$^+$/$TiO_2(e^-)$ → **Dye-O**/$TiO_2$ recombination as the number of electrons trapped in $TiO_2$ was raised toward the values expected at the open circuit condition. Below we discuss these two key findings in regard to the interfacial energetics, kinetics, and conversion efficiency in dye-sensitized solar cells.

**Interfacial Energetics.** Spectroelectrochemistry of the sensitized thin films revealed that the electrochemical reduction of $TiO_2$ was insensitive to the identity of the surface anchored dye molecules. Reduction of $TiO_2$ results in a blue-black coloration of the film that has been attributed to trapped $TiO_2(e^-)$'s, most probably as $Ti^{III}$ sites.[31] Employing the approach of Bisquert and co-workers,[32] the potential-dependent redox chemistry was converted to a chemical capacitance. A key assumption was that electrons could be independently added and removed from the $TiO_2$; that is, the electrons are screened from each other. With this assumption, molecular excited states with reduction potentials as low as 0 V vs NHE would be able to inject electrons into $TiO_2$, Figure 10. **Dye-O** and **Dye-S** are much more potent reductants, and quantitative injection was expected. The knowledge that the $E(S^+/S^*)$ potential is ~600 mV higher than needed for efficient electron injection allows for future work on developing these sensitizers by extending the $\pi$-bridge to lower the $E(S^+/S^*)$ and consequently covering a larger portion of the solar spectrum.

The dye molecules could be reversibly oxidized, and the potential dependence is displayed in the form of chemical capacitance. The peak of the distributions shown corresponds to the potential where equal concentrations of the oxidized and reduced forms were present. This value was taken as the formal reduction

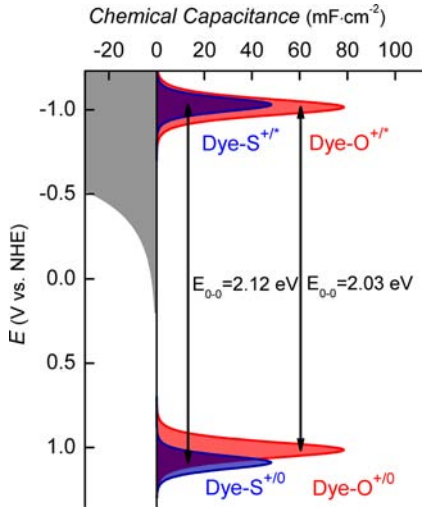


**Figure 10.** Interfacial energetics of **Dye-O**/$TiO_2$ and **Dye-S**/$TiO_2$ in 0.5 M $LiClO_4/CH_3CN$ solution.

potential and was found to be 75 mV more positive for **Dye-S**/$TiO_2$ than for **Dye-O**/$TiO_2$. This difference was attributed to the poorer orbital overlap of the lone pair of the sulfur atom with the phenyl ring.[20] Nevertheless, measurements of the photovoltage generated in the absence of redox mediators showed that the free energy stored in the **Dye-O**$^+$/$TiO_2(e^-)$ and **Dye-S**$^+$/$TiO_2(e^-)$ interfacial charge-separated states were within experimental error the same. Taken together, these data indicate that the change of heteroatoms did not appreciably influence interfacial thermodynamics for **Dye-O**/$TiO_2$ and **Dye-S**/$TiO_2$.

**Interfacial Kinetics.** Charge recombination between the injected $TiO_2(e^-)$ and the oxidized dye molecules was within experimental error the same for both **Dye-O**/$TiO_2$ and **Dye-S**/$TiO_2$. This observation was expected as the driving force for the


dx.doi.org/10.1021/ja311640f | J. Am. Chem. Soc. 2013, 135, 1961−1971

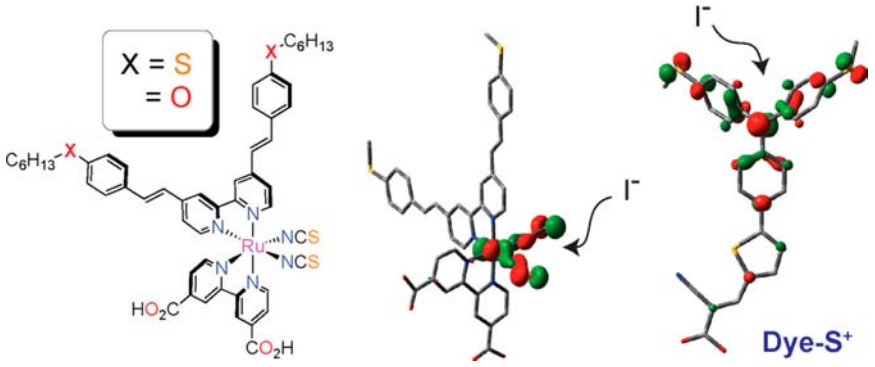


**Figure 11.** Molecular structures of two ruthenium(II)-based dyes studies by O'Regan and co-workers[10] indicating the site where the heteroatoms have been changed. The $\beta$-LUSO (lowest-unoccupied spin orbital) for the oxidized form of the ruthenium dye where X = S is shown to the left of the $\beta$-LUSO for **Dye-S**$^+$ (also shown in Figure 1) to highlight that there is no orbital character over the S atoms in the metal dye and significant orbital character over the S atoms in the organic dye. The portions of the respective dyes that ostensibly interact with the redox mediator are illustrated. The equivalent spin-density plots are found in Figure S15.

reactions differed by merely 75 mV.[33,34] The average rate constants, $k_{cr}$, abstracted from a distributional analysis of the kinetic data were highly sensitive to the presence of excess $TiO_2(e^-)$'s. This behavior was first recognized by Durrant and co-workers for *cis*-Ru(4,4′-dicarboxy-2,2′-bipyridine)$_2$(NCS)$_2$/$TiO_2$[35] and was immediately apparent for the organic dyes studied herein. The $k_{cr}$ values increased exponentially with the applied forward bias that, given the exponential density of states known for $TiO_2$, implies a reaction that is first-order in $TiO_2(e^-)$ concentration.

The kinetics for sensitizer regeneration were quantified spectroscopically. With $[Co(bpy)_3]^{2+}$ as the electron donor, second-order rate constants of the order of $10^6$ $M^{-1}\cdot s^{-1}$ were measured for reaction 6.

$$\textbf{Dye-X}^+/TiO_2 + Co^{II}(bpy)_3^{2+} \rightarrow \textbf{Dye-X}/TiO_2(e^-) + Co^{III}(bpy)_3^{3+} \quad (\textbf{X} = \textbf{O or S}) \tag{6}$$

At high $[Co(bpy)_3]^{2+}$ concentrations (i.e., above 0.13 M) and low concentrations of trapped $TiO_2(e^-)$'s, the regeneration step was quantitative, consistent with the high photocurrent efficiencies measured at the short circuit condition. The high photocurrents also indicated that the unwanted charge recombination of the injected electron with the oxidized cobalt compound, $[Co(bpy)_3]^{3+}$, was inefficient. This observation likely emanates from the well-known spin change that accompanies $Co^{III/II}$ redox chemistry that results in anomalously small self-exchange rate constants.[36,37] The $[Co(bpy)_3]^{2+}$ compound has a $d^7$ high spin electron configuration ($t_{2g}^5e_g^{*2}$), and $[Co(bpy)_3]^{3+}$ has a $d^6$ low-spin configuration ($t_{2g}^6$). Consistent with other sensitizers that have displayed high solar conversion efficiencies with a $Co^{III/II}$ redox mediator, the long hexyl hydrocarbon chains of the dye molecules are postulated to effectively shield the $TiO_2$ surface from the $[Co(bpy)_3]^{3+}$.[2]

Iodide oxidation has been the subject of many studies[38,39] and occurs by two different mechanisms: one that is first-order in iodide to generate the iodine atom; and the other that is second-order in iodide to yield an iodine radical anion called di-iodide, $I_2^{\bullet-}$. It remains unclear which mechanism(s) are operative at sensitized $TiO_2$ interfaces. This ambiguity is due in part to the rapid reactivity of the iodine atom with iodide to yield the same $I_2^{\bullet-}$ product. However, the latter mechanism is generally thought to be operative in solar cells as the thermodynamics for this outer-sphere electron transfer pathway are more favorable.[6] For example, the free energy change for regeneration of the classical **N3** sensitizer, *cis*-Ru(dcb)$_2$(NCS)$_2$, to yield the iodine atom is endergonic by +140 mV ($E°(I^\bullet/I^-)$ =1.23 V vs NHE), while it is exergonic by −160 mV for $I_2^{\bullet-}$ formation ($E°(I_2^{\bullet-}/2I^-)$ = 0.93 V vs NHE).[40] The corresponding driving forces for regeneration of **Dye-S**/$TiO_2$ studies here are essentially identical, suggesting specific interactions between the oxidized dye and iodide. While these arguments are not definitive as inner-sphere dye−iodide adducts may activate iodide and significantly alter the thermodynamics,[41] ion-pairing with the oxidized dye is generally invoked to explain regeneration mechanisms at sensitized $TiO_2$ interfaces, reaction 7.[42]

$$[I^-, \textbf{Dye-X}^+/TiO_2] + I^- \rightarrow \textbf{Dye-X}/TiO_2 + I_2^{\bullet-} \quad (\textbf{X} = \textbf{O or S}) \tag{7}$$

In the present case, the rate constant for regeneration differs by a factor of 25 with only a 75 mV change in driving force for **Dye-O**$^+$ and **Dye-S**$^+$. This finding is striking in that previous kinetic data indicate that a 75 mV change in driving force would not have such a dramatic influence on the electron transfer rate constant.[11,30] For example, Palomares and co-workers observed a 4-fold enhancement of regeneration with an additional 60 mV driving force,[11] while O'Regan and co-workers observed a 20-fold enhancement of regeneration with over 300 mV driving force.[43] Clearly the dependence of the measured electron transfer rate constants on $-\Delta G$ will be a function of where they sit on the Marcus parabola. Reactions that occur near the top of the parabola, that is, where $-\Delta G = \lambda$, may show a very shallow $\Delta G$ dependence, whereas those that are highly unfavored show a stronger dependence. Nevertheless, a 25-fold change in rate constant cannot reasonably be attributed to only a 75 mV change in driving force.

Inspection of the molecular orbitals of the two dyes reveals a higher orbital coefficient on the S atom relative to the O atom. This description is more predominant in the oxidized forms of the dyes, which is the more relevant form to be considered here. **Dye-O** and **Dye-S** offer the first examination of how different heteroatoms affect the regeneration step, where the heteroatoms constitute the portion of the molecule that will be interacting with the electrolyte. Previous studies on the heteroatom effect in coordination compounds placed the heteroatom on a remote portion of a bipyridine ligand, Figure 11. Consequently, this resulted in differences in behavior that were manifest in the recombination step, but not necessarily the regeneration step. The reaction between the oxidized forms of **Dye-O** and **Dye-S** and the redox mediator will almost certainly involve the portion


dx.doi.org/10.1021/ja311640f | *J. Am. Chem. Soc.* 2013, 135, 1961−1971

of the molecule bearing the triaryl fragment containing the heteroatoms of interest. Consequently, the much faster rates of dye regeneration provide incontrovertible evidence that the S atoms mediate an interaction with the redox mediator that is favorable relative to the O atoms. Adduct formation between iodide and the soft more polarizable sulfur atom as the Lewis base at the regeneration site would provide an inner-sphere electron transfer pathway that could enhance electronic coupling and hence alter the electronic transmission coefficient. Alternatively, the higher rate of the reaction could simply be a result of the greater orbital coefficient on the S atom on the O atom.

In either event, transient absorption data clearly show that the unwanted charge recombination reaction with oxidized iodide species was not influenced by the presence of the sulfur atoms positioned near the donor site of these organic dyes as was invoked previously for the ruthenium-based sensitizers.[10] Recombination of the injected electrons with $I_3^-$ or $I_2$ was within experimental error the same for the two dye-sensitized $TiO_2$ materials, 2.3 ± 0.4 $s^{-1}$. Di-iodide, an intermediate in the regeneration reaction and a $I_3^-$ reduction product, is also a potential electron acceptor,[44,45] yet there was no evidence for a reaction between **Dye-S**/$TiO_2(e^-)$ and $I_2^{\bullet-}$. Instead, the $I_2^{\bullet-}$ formed during regeneration underwent disproportionation with a quantum yield and reaction rate constant that was unchanged from that measured in fluid acetonitrile solution.[28]

The question remains whether more rapid regeneration by **Dye-S**$^+$/$TiO_2(e^-)$ could account for the larger open circuit photovoltage, $V_{oc}$, measured in the DSSCs. Generally speaking, the observation of quantitative short circuit photocurrents and IPCE values has led previous authors to conclude that regeneration is optimal.[7] However, at short circuit the injected electrons are rapidly removed from $TiO_2$ thin film, whereas at the open circuit condition many electrons are trapped within each nanocrystallite, behavior that is known to enhance charge recombination.[35] Indeed, as electrons were thermally transferred to $TiO_2$ with an external potentiostat, recombination to these oxidized organic dyes increased significantly and the corresponding regeneration efficiency decreased. At −200 mV vs NHE, the regeneration efficiency for **Dye-S**$^+$/$TiO_2(e^-)$ was near unity for both donors, while that for **Dye-O**$^+$/$TiO_2(e^-)$ had dropped by about 20% for iodide and 40% for $Co(bpy)_3^{2+}$. The more significant decrease for the cobalt mediator reflects the fact that it did not regenerate as quickly as did iodide. These regeneration efficiencies explain the smaller $V_{oc}$ values measured for **Dye-O** as well as it is greater sensitivity to the cobalt mediator as is described more fully below.

Correlations of measurements made under potentiostatic conditions with an operational solar cell are nontrivial. Ideally, one would like to employ transient absorption spectroscopy directly as an in situ characterization tool for DSSCs as has been done in pioneering studies by O'Regan and co-workers.[46,47] However, transmission losses associated with the complete DSSC coupled with the necessary corrections for redox chemistry that occurs at the counter electrode have thus far precluded data of the quality presented herein. Nevertheless, about 20 electrons have been calculated to reside in each $TiO_2$ nanocrystallite at the power point, albeit a value noted to be quite sensitive to the distribution of $TiO_2$ particle sizes.[46] With reasonable assumptions of extinction coefficient and path length, the measured $TiO_2(e^-)$ absorption at −200 mV is in good agreement with this value, and the number would be even higher at the open circuit condition. Thus, the potentiostatic kinetic data provide compelling evidence that the high short circuit photocurrents for both dyes are due to quantitative regeneration and the low $V_{oc}$ value for **Dye-O**/$TiO_2$ results from poor regeneration when the $TiO_2(e^-)$ concentration is high. Hence, the detailed mechanistic studies reported herein show that the observation of quantitative short circuit photocurrents is not necessarily an indication that regeneration is optimal. Quantitative regeneration of **Dye-S**$^+$/$TiO_2$ as the $TiO_2(e^-)$ concentration was raised toward the values expected at the open circuit condition underlies its superior performance and $V_{oc}$ values relative to **Dye-O**/$TiO_2$.

## ■ CONCLUSIONS

To our knowledge, this study provides the first direct comparison of molecules where a simple two-atom change, at the site of regeneration, systematically probes the rates of regeneration by $I^-$ (and Co(II)). The results of this study contrast the broadly accepted view that S atoms enhance the rate of recombination between the $TiO_2(e^-)$ and the oxidized iodide mediator, thus lowering the solar conversion efficiency of the DSSC. These disparities in reactivities are manifest in the specific positioning of the heteroatom change within the portion of the dye molecule that is most likely to react with the incoming reductant $I^-$. These results highlight that the atomic composition of the dye can have a profound effect on the dye regeneration process, and that the careful design of molecular dyes can lead to an optimization of interactions with the redox mediator that can lead to further enhancements in dye regeneration. Furthermore, the data provide compelling evidence that sluggish regeneration can lower the open circuit photovoltage even when quantitative short circuit photocurrents are measured.

## ■ ASSOCIATED CONTENT

### Supporting Information

Synthetic details, physical methods, and spectroscopic, electrochemical, and computational data. This material is available free of charge via the Internet at http://pubs.acs.org.

## ■ AUTHOR INFORMATION

### Corresponding Author

meyer@jhu.edu; cberling@ucalgary.ca

### Notes

The authors declare no competing financial interest.

## ■ ACKNOWLEDGMENTS

K.H. and G.J.M. acknowledge support by a grant from the Division of Chemical Sciences, Office of Basic Energy Sciences, Office of Energy Research, U.S. Department of Energy (DE-FG02-96ER14662). C.P.B. and K.C.D.R. are grateful to the Canadian Natural Science and Engineering Research Council, Canadian Foundation for Innovation, Alberta Ingenuity, Canada School of Energy and Environment (CSEE); and the Alfred P. Sloan Foundation for support.

## ■ REFERENCES

(1) O'Regan, B.; Grätzel, M. *Nature* **1991**, *353*, 737−740.
(2) Yella, A.; Lee, H. W.; Tsao, H. N.; Yi, C.; Chandiran, A. K.; Nazeeruddin, M. K.; Diau, E. W. G.; Yeh, C. Y.; Zakeeruddin, S. M.; Grätzel, M. *Science* **2011**, *334*, 629−634.
(3) Yum, J.-H.; Baranoff, E.; Kessler, F.; Moehl, T.; Ahmad, S.; Bessho, T.; Marchioro, A.; Ghadiri, E.; Moser, J.-E.; Yi, C.; Nazeeruddin, M. K.; Grätzel, M. *Nat. Commun.* **2012**, *3*, 631−633.
(4) Bomben, P. G.; Gordon, T. J.; Schott, E.; Berlinguette, C. P. *Angew. Chem., Int. Ed.* **2011**, *50*, 10682−10685.

(5) Feldt, S. M.; Gibson, E. A.; Gabrielsson, E.; Sun, L.; Boschloo, G.; Hagfeldt, A. *J. Am. Chem. Soc.* **2010**, *132*, 16714−16724.
(6) Boschloo, G.; Hagfeldt, A. *Acc. Chem. Res.* **2009**, *42*, 1819−1826.
(7) Ardo, S.; Meyer, G. J. *Chem. Soc. Rev.* **2009**, *38*, 115−164.
(8) Clifford, J. N.; Martinez-Ferrero, E.; Viterisi, A.; Palomares, E. *Chem. Soc. Rev.* **2011**, *40*, 1635−1646.
(9) Liu, F.; Meyer, G. J. *J. Am. Chem. Soc.* **2004**, *127*, 824−825.
(10) O'Regan, B. C.; Walley, K.; Juozapavicius, M.; Anderson, A.; Matar, F.; Ghaddar, T.; Zakeeruddin, S. M.; Klein, C. d.; Durrant, J. R. *J. Am. Chem. Soc.* **2009**, *131*, 3541−3548.
(11) Planells, M.; Pelleja, L.; Clifford, J. N.; Pastore, M.; De Angelis, F.; Lopez, N.; Marder, S. R.; Palomares, E. *Energy Environ. Sci.* **2011**, *4*, 1820−1829.
(12) Reynal, A.; Forneli, A.; Martinez-Ferrero, E.; Sánchez-DÍaz, A.; Vidal-Ferran, A. N.; O'Regan, B. C.; Palomares, E. *J. Am. Chem. Soc.* **2008**, *130*, 13558−13567.
(13) Hu, K.; Robson, K. C. D.; Johansson, P. G.; Berlinguette, C. P.; Meyer, G. J. *J. Am. Chem. Soc.* **2012**, *134*, 8352−8355.
(14) Li, R.; Lv, X.; Shi, D.; Zhou, D.; Cheng, Y.; Zhang, G.; Wang, P. *J. Phys. Chem. C* **2009**, *113*, 7469−7479.
(15) Mishra, A.; Fischer, M. K. R.; Bäuerle, P. *Angew. Chem., Int. Ed.* **2009**, *48*, 2474−2499.
(16) Zeng, W.; Cao, Y.; Bai, Y.; Wang, Y.; Shi, Y.; Zhang, M.; Wang, F.; Pan, C.; Wang, P. *Chem. Mater.* **2010**, *22*, 1915−1925.
(17) Hagberg, D. P.; Edvinsson, T.; Marinado, T.; Boschloo, G.; Hagfeldt, A.; Sun, L. *Chem. Commum.* **2006**, 2245−2247.
(18) Robson, K. C. D.; Koivisto, B. D.; Yella, A.; Sporinova, B.; Nazeeruddin, M. K.; Baumgartner, T.; Gratzel, M.; Berlinguette, C. P. *Inorg. Chem.* **2011**, *50*, 5494−5508.
(19) Karthikeyan, C. S.; Wietasch, H.; Thelakkat, M. *Adv. Mater.* **2007**, *19*, 1091−1095.
(20) Robson, K. C. D.; Koivisto, B. D.; Berlinguette, C. P. *Inorg. Chem.* **2012**, *51*, 1501−1507.
(21) Dienes, Y.; Durben, S.; Karpati, T.; Neumann, T.; Englert, U.; Nyulaszi, L.; Baumgartner, T. *Chem.-Eur. J.* **2007**, *13*, 7487−7500.
(22) Bonhote, P.; Dias, A.-P.; Papageorgiou, N.; Kalyanasundaram, K.; Gratzel, M. *Inorg. Chem.* **1996**, *35*, 1168−1178.
(23) Argazzi, R.; Bignozzi, C. A.; Heimer, T. A.; Castellano, F. N.; Meyer, G. J. *Inorg. Chem.* **1994**, *33*, 5741−5749.
(24) Frisch, M. J.; et al. *Gaussian 03*, revision C.02; Gaussian, Inc.: Wallingford, CT, 2004.
(25) Ardo, S.; Sun, Y.; Staniszewski, A.; Castellano, F. N.; Meyer, G. J. *J. Am. Chem. Soc.* **2010**, *132*, 6696−6709.
(26) Cappel, U. B.; Feldt, S. M.; Schoneboom, J.; Hagfeldt, A.; Boschloo, G. *J. Am. Chem. Soc.* **2010**, *132*, 9096−9101.
(27) Williams, G.; Watts, D. C. *Trans. Faraday Soc.* **1970**, *66*, 3348−3358.
(28) Lindsey, C. P.; Patterson, G. D. *J. Chem. Phys.* **1980**, *73*, 3348−3357.
(29) Rowley, J. G.; Ardo, S.; Sun, Y.; Castellano, F. N.; Meyer, G. J. *J. Phys. Chem. C* **2011**, *115*, 20316−20325.
(30) Bai, Y.; Zhang, J.; Zhou, D.; Wang, Y.; Zhang, M.; Wang, P. *J. Am. Chem. Soc.* **2011**, *133*, 11442−11445.
(31) Boschloo, G.; Fitzmaurice, D. *J. Electrochem. Soc.* **2000**, *147*, 1117−1123.
(32) Bisquert, J.; Fabregat-Santiago, F.; Mora-Seró, I.; Garcia-Belmonte, G.; Barea, E. M.; Palomares, E. *Inorg. Chim. Acta* **2008**, *361*, 684−698.
(33) Clifford, J. N.; Palomares, E.; Nazeeruddin, M. K.; Grätzel, M.; Nelson, J.; Li, X.; Long, N. J.; Durrant, J. R. *J. Am. Chem. Soc.* **2004**, *126*, 5225−5233.
(34) Hasselmann, G. M.; Meyer, G. J. *J. Phys. Chem. B* **1999**, *103*, 7671−7675.
(35) Haque, S. A.; Tachibana, Y.; Klug, D. R.; Durrant, J. R. *J. Phys. Chem. B* **1998**, *102*, 1745−1749.
(36) Rillema, D. P.; Endicott, J. F. *Inorg. Chem.* **1972**, *11*, 2361−2366.
(37) Sutin, N.; Creutz, C. *J. Chem. Educ.* **1983**, *60*, 809.
(38) Nord, G. *Comments Inorg. Chem.* **1992**, *13*, 221−239.
(39) Wang, X.; Stanbury, D. M. *Inorg. Chem.* **2006**, *45*, 3415−3423.
(40) Rowley, J. G.; Farnum, B. H.; Ardo, S.; Meyer, G. J. *J. Phys. Chem. Lett.* **2010**, *1*, 3132−3140.
(41) Farnum, B. H.; Jou, J. J.; Meyer, G. J. *Proc. Natl. Acad. Sci. U.S.A.* **2012**, *109*, 15629−15633.
(42) Clifford, J. N.; Palomares, E.; Nazeeruddin, M. K.; Grätzel, M.; Durrant, J. R. *J. Phys. Chem. C* **2007**, *111*, 6561−6567.
(43) Martiniani, S.; Anderson, A. Y.; Law, C.; O'Regan, B. C.; Barolo, C. *Chem. Commun.* **2012**, *48*, 2406−2408.
(44) Farnum, B. H.; Gardner, J. M.; Meyer, G. J. *Inorg. Chem.* **2010**, *49*, 10223−10225.
(45) Bauer, C.; Boschloo, G.; Mukhtar, E.; Hagfeldt, A. *J. Phys. Chem. B* **2002**, *106*, 12693−12704.
(46) O'Regan, B. C.; Durrant, J. R. *Acc. Chem. Res.* **2009**, *42*, 1799−1808.
(47) Anderson, A. Y.; Barnes, P. R. F.; Durrant, J. R.; O'Regan, B. C. *J. Phys. Chem. C* **2010**, *114*, 1953−1958.